Ceramics International 23 (1997) 463–469

PII: S0272-8842(96)00054-5
0272-8842/97 $17.00+.00

Lithia Porcelains as Promising Breeder Candidates — I. Preparation and Characterization of β-Eucryptite and β-Spodumene Porcelain

Wafa I. Abdel-Fattah[a] & R. Abdellah[b]

[a]National Research Centre, Ceramic Department, Dokki, Cairo, Egypt
[b]Faculty of Industrial Education, Helliopolis, Cairo, Egypt

(Received 20 November 1995; accepted 9 April 1996)

Abstract: β-Eucryptite, β-spodeumene and solid-solution porcelain were prepared by the conventional ceramic technique with three lithia:alumina:silica (LAS) ratios, 1:1:2, 1:1:3 and 1:1:4. The optimization of the ceramic parameters was assessed through measuring their vitrification parameters with firing temperatures in the range 1000–1350 °C. Structural characterization of the bodies obtained at optimum conditions were followed through X-ray diffraction (XRD) and infrared (IR) spectral analyses. Thermal dilation up to 1000 °C was measured. Morphological variations were examined through scanning electron microscopy (SEM) of fractured surfaces, as well as selected area electron diffraction (SAED).

Results proved that the change from β-eucryptite with 1:1:2 LAS through its solid solution to β-spodumene with 1:1:4 LAS, i.e. from hexagonal to tetragonal structures, need a firing temperature of 1320 °C. Shifts in XRD lattice planes were complemented by parallel shifts in IR bands specific for silicates around 1100 cm^{-1}. Unique negative thermal expansion up to 1000 °C for β-eucryptite changed to the positive value only after 600 °C for β-spodumene. Characteristic large grains were detected in both β-eucryptite and β-spodumene micrographs parallel with the polycrystalline rings of the SAED figures. On the other hand, the β-eucryptite solid-solution body has smaller grain size with higher glassy phase shown by the larger SAED halo. The present results illuminate the importance of assessing the detailed structural features for future radiation damage studies. © 1997 Elsevier Science Limited and Techna S.r.l.

1 INTRODUCTION

The technical use of new materials based on the lithia–alumina–silica system lies, so far, in the areas of high temperature gradients, rapid temperature changes and neutron fluences. They are under evaluation for recent application in automotive ceramic gas turbine engines, which require materials to be used in regenerator cores that salvage waste heat for improved fuel consumption.[1] Lithia porcelains are also reported for their low sensitivity to low fast neutron fluences,[2] that could satisfy several requirements for solid breeder materials to generate and recover both tritium and heat in the fusion reactor blanket.[3] β-Eucryptite and β-spodumene are quartz derivatives, where the former has a hexagonal bi-pyramidal structure and the latter is di-tetragonal bi-pyramidal, with two solid-solutions in between.[4–6] The mineralogical, chemical and physical properties of the raw materials, as well as the technique of preparing and firing lithia minerals, were studied to determine whether the product has positive or negative expansion.[7] In open silicate systems, hydrogen bonding should be considered carefully, in radiation field applications where radiolysis may result in atom displacements.[8] Radiation-induced hole centres are enhanced with the presence of as little as 0.01% OH.[9]

The present work deals with the preparation, vitrification and characterization of porcelains of β-eucryptite, β-spodumene and a solid-solution in between. Thermal expansion and/or contraction up to 1000 °C are followed. Detailed structural assessment including X-ray diffraction and infrared analyses are supplemented by scanning electron microscopy of fractured surfaces and selected area electron diffraction (SAED) of their powders.

2 EXPERIMENTAL PROCEDURE

2.1 Lithia porcelain

Three porcelain compositions along the field of eucryptite–spodumene crystallization were prepared (see Table 1). The compositions covered those of eucryptite LAS1 ($Li_2O.Al_2O_3.2SiO_2$) and spodumene LAS3 ($Li_2O.Al_2O_3.4SiO_2$) to induce negative and positive thermal expansion, respectively.[10] Chemically pure lithium carbonate (99.5)(Riedel-De Haenag Seelze, Hannover) and local quartz (99.83% SiO_2)(Aswan, upper Egypt) were used. Pure kaolin ($Al_2O_3.2SiO_2.2H_2O$) (Montecatens. E.A. Milan, Italy) was used as a source of Al_2O_3 and SiO_2.

Proper percentages of ingredients were thoroughly wet, mixed, dried and calcined with 10 °C min^{-1} heating rate and 1/2 h soaking at 950 °C. The calcined powders were finely ground to give powders with 12 m^2/g surface area. The green (unfired) specimens were shaped by semi-dry pressing with 5% solution carbowax 800 as a binder. The pressure used was 100 kg/cm^2 (automatically controlled hydraulic press, Seider type LP800 M1, West Germany).

2.2 Vitrification

The pressed specimens were air and oven dried successively for 24 h each. Firing was conducted in an automatic chamber furnace (model 20/H with temperature processor TPI-Naber, West Germany) at various temperatures in the range 1000–1350 °C at 20 °C intervals and a heating rate of 5 °C/min to obtain the range curves. The vitrification parameters of the specimens were measured (ASTM 1981). True porosity was calculated from the relation:

$$\text{True porosity} = SG - BD/SG \times 100\%$$

where SG = specific gravity determined for the powders of vitrified specimens using Dekalin as an immersion media and a standard pyknometer and BD = bulk density (g/cm^3).

Table 1. Compositions of the three lithia porcelains

Body notation	Mole ratio L.A.S.	Oxide composition (wt%)			Batch composition (wt%)		
		Li_2O	Al_2O_3	SiO_2	Li_2CO_3	Kaolin	Quartz
LAS1	1:1:2	11.86	40.46	47.68	22.25	77.75	—
LAS2	1:1:3	9.57	32.67	57.76	18.83	65.84	15.33
LAS3	1:1:4	8.03	27.39	64.58	16.34	57.07	26.59

2.3 Thermal changes

A horizontal vitreous silica dilatometer (J. Malkia and Co. Ltd product, Stoke-on-Trent, UK) calibrated using standard fused silica (NBS 739) was used up to 1000 °C with a heating rate of 3–5 °C/min.

2.4 Structural assessment

X-ray powder diffraction (Dyano Diffractometer 8000) was used to detect the developed phases at a scanning speed of 0.2θ/min. and CuKα radiation. Infrared analysis using the KBr disc technique (1:100) was used (Unicom-SP/1000 Spectrophotometer). A scanning electron microscope was

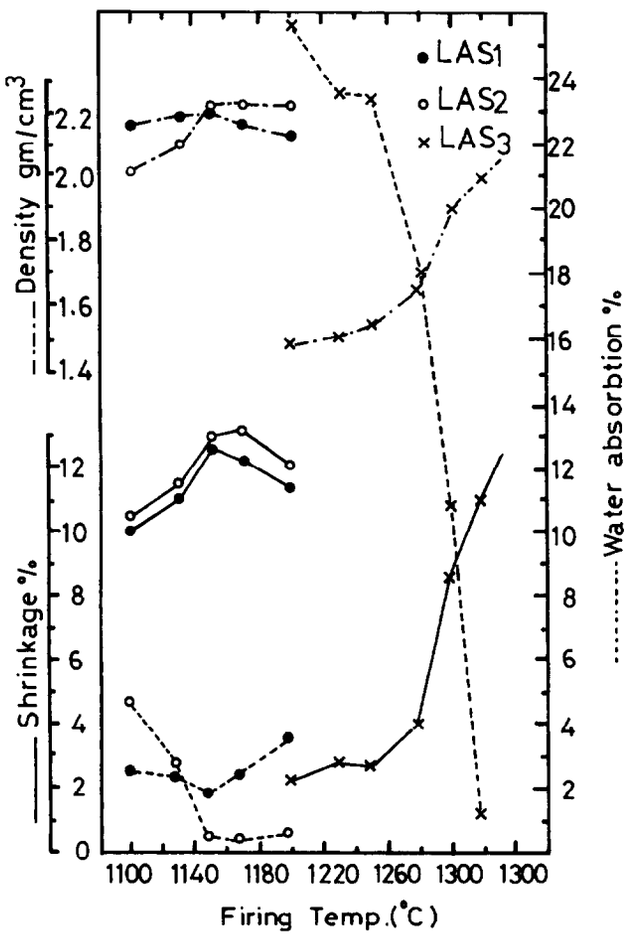

Fig. 1. Vitrification of lithia ceramic bodies.

used to examine the fracture surface after sputtering with gold (Joel). Selected area electron diffraction (SAED) of the powders was studied using a transmission electron microscope operating at 45 kV (Elmi D_2, Carl Zeiss, Jena, L = 21.75Å).

3 RESULTS AND DISCUSSION

3.1 Vitrification

Specimens of LAS1 and LAS2 exhibited the same general features, both being liable to sinter at much lower temperature compared to LAS3 and possessing maxima turning points in their property curves (Fig. 1). LAS3 specimens attained their properties at a higher temperature (1320 °C) with a sudden vitrification denoting a short firing range. The distortion of the specimens above 1320 °C is due to excessive melting and a sudden drop in the viscosity of the developed glassy phase, especially at higher temperatures.

Zero porosity and complete vitrification are attained with LAS2. Higher lithia and alumina or silica contents led to higher porosities.

3.2 Structural analyses

3.2.1 X-ray diffraction analysis

The patterns of LAS1 specimens (Fig. 2) are characteristic of pure β-eucryptite ($Li_2O.Al_2O_3.2SiO_2$), while those of LAS3 are of β-spodumene ($Li_2O.Al_2O_3.4SiO_2$) (Fig. 2), with some similarities between them. The LAS2 patterns show great similarity to those of β-eucryptite but with some shift of the most intense line (Fig. 2), suggesting a solid-solution.[11]

3.2.2 Infrared analysis

A small shift in the absorption band positions within the 4000–1300 cm^{-1} range characteristic of $(OH)^-$ and water species,[12] was detected, while the shift below 1300 cm^{-1}, characteristic for aluminosilicates,[13] is considerable (Fig. 3). At higher lithia content, $(OLi)^-$ sites were detected at 3500 cm^{-1}, which is reduced as the system changes to the tetragonal symmetry (i.e. β-spodumene), where room for $(OLi)^-$ or $(OH)^-$ accommodation is less available. It seems that chemically trapped water (3100 cm^{-1}) is less important than physically trapped water (3400 cm^{-1}) between the planes. Both

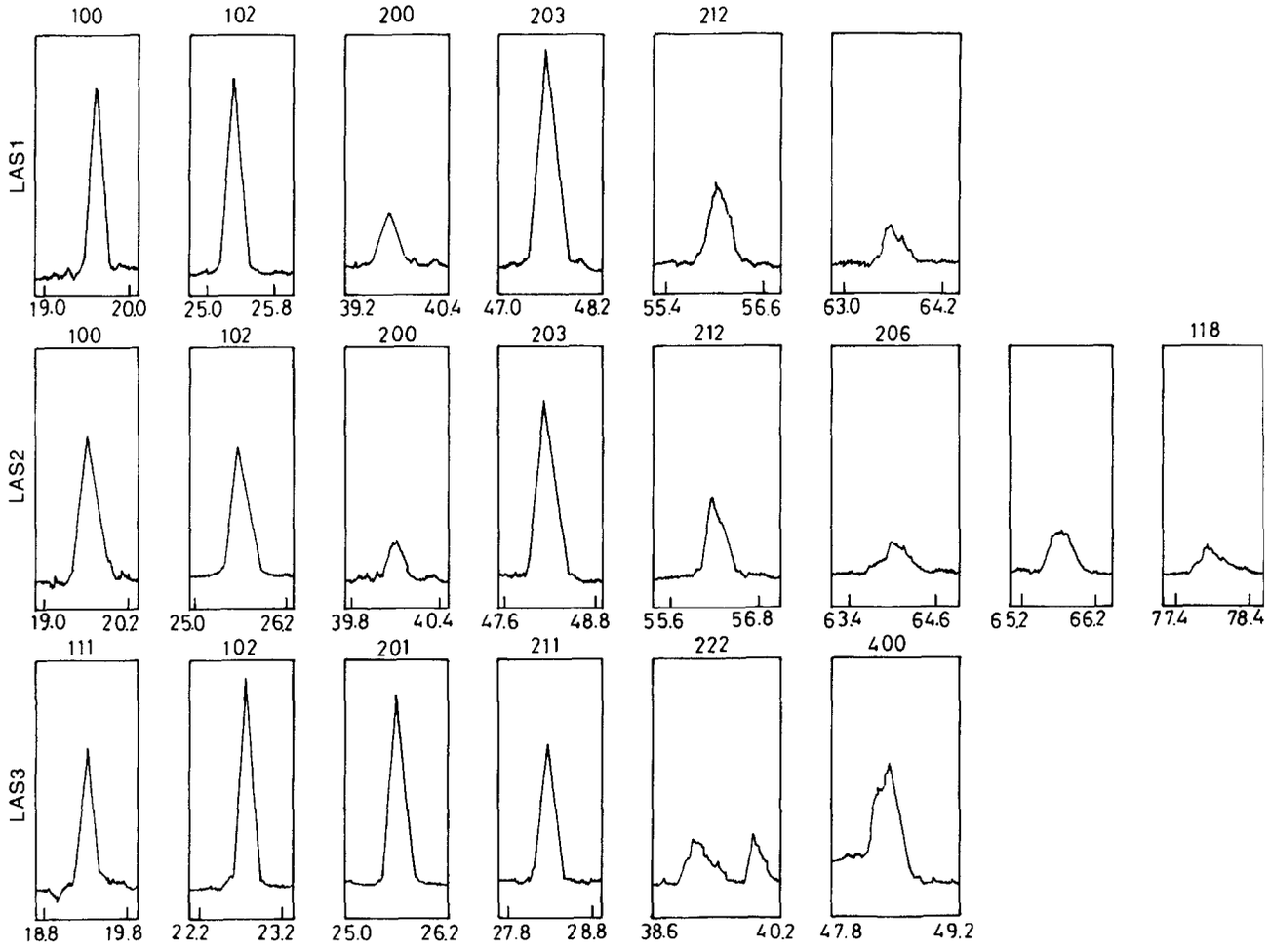

Fig. 2. XRD traces of the characteristic lithia phases (lattice planes).

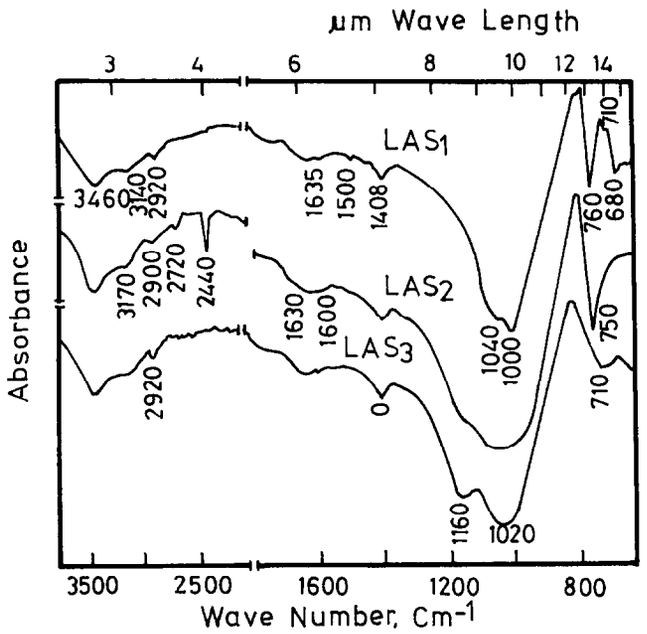

Fig. 3. Infrared spectral analysis of lithia ceramic bodies.

1635 cm^{-1} (H–O–H) and 1430 cm^{-1} (assigned for absorbed water) have reduced intensity going from LAS1 to LAS3 through LAS2. The progressive shift in the silicate region is parallel with the reduced alumina content, notably reducing $(AlO_4)^-$ and $(AlO_6)^-$ bands. The intensity of the 9.8 μm band decreased with increasing SiO_2/Al_2O_3 ratio in parallel with a decrease in the intensity of the 13.3 μm band. The vibrations of AlO_4 and SiO_4 are similar, but due to the larger size of AlO_4 and the lower field strength of the Al^{3+} ion, the frequency of AlO_4 would be lower than for SiO_4. If both groups are present, interference of two or more bands will occur resulting in a decrease or increase of the intensity of a certain band.

3.3 Thermal changes

Below 250 °C the thermal contraction of LAS1 (Fig. 4) could be due to contraction along the *c*-axis, as it was reported to be associated with transverse vibrations with oxygen atoms in the open network.[14] Such negative expansion would be reduced and becomes positive with increasing silica content (LAS2) and with the formation of β-spodumene (LAS3) (Fig. 5). The low thermal expansion of these materials is reported to be composition and structure dependant.[15] The temperature regions of stable dimensions are at higher range, the higher the LAS ratio. Stable expansion values (L_T%) within the 150–275 °C range followed the order 0.016 > 0.008 > 0.001 for LAS1 > LAS2 > LAS3, respectively. Regions of expansion stability, where $\Delta L(L_T - L_{T0})$ = constant, in spite of raising the temperature, are related to an order–disorder transition (Fig. 6). Schulz[16] recorded this transition for β-eucryptite to be at 460 °C. Superstructure reflections were reported to decrease continuously in intensity and above 460 °C become unobservable, denoting ion splitting.[17] Zero expansion temperature, where bodies regained their original length due to Li-hopping accom-

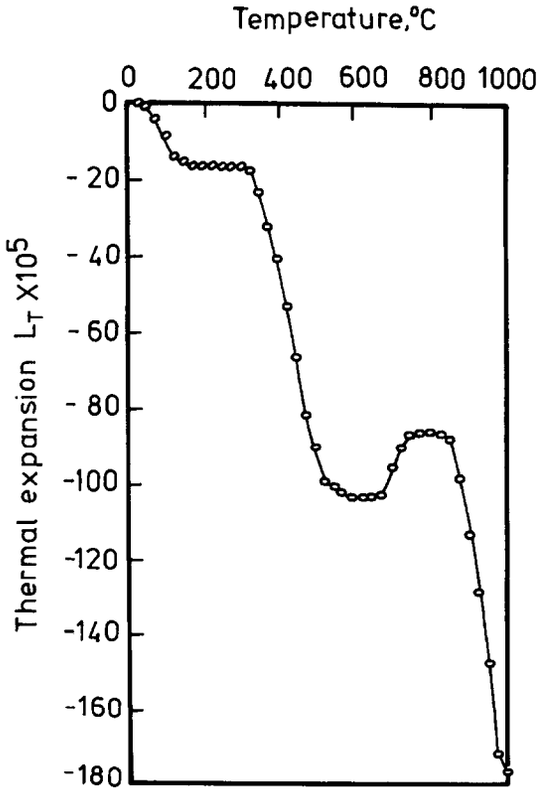

Fig. 4. Thermal contraction of β-eucryptite ceramic.

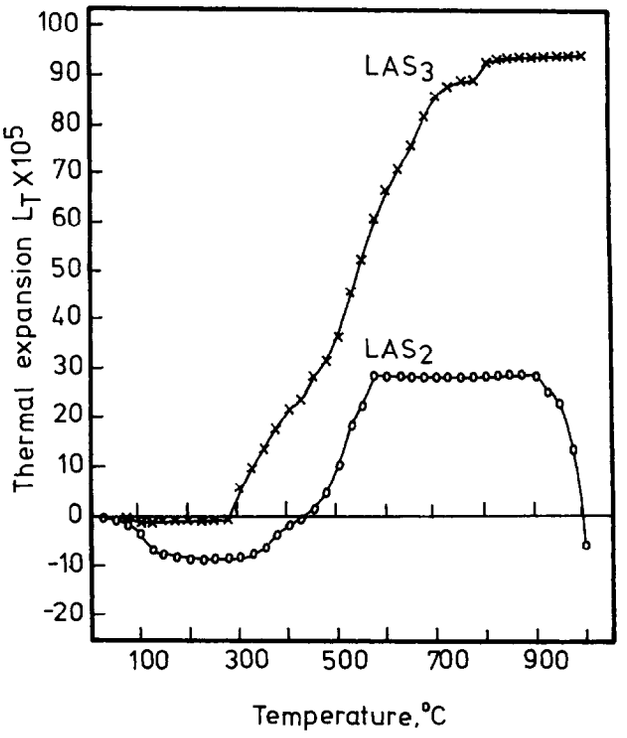

Fig. 5. Thermal contraction and expansion of β-eucryptite solid-solution and β-spodumene ceramic.

panying the order–disorder transition, occurred at higher temperatures in parallel with higher silica content, i.e. because of reduced anisotropy and lower internal stresses.[18] Zero expansion temperature (T_z) for β-spodumene was recorded to be at 400 °C.[19] The values of negative and positive coefficient of linear thermal expansion from the present study are shown below.

$\alpha_{75}^{150}\times10^{-7}$			$\alpha_{500}^{575}\times10^{-7}$		
LAS1	LAS2	LAS3	LAS1	LAS2	LAS3
−14.7	−8	−1.3	−23.7	+24	+32

3.4 Microtopography

3.4.1 Fracture surface

The scanning electron microscopy revealed a higher degree of crystallinity in both LAS1 and LAS2 [Fig. 7(a) and (c)]. Hexagonal β-eucryptite structure dominates in Fig. 7(b) LAS1. Enlarged sub-hedral grains [Fig. 7(f)] are characteristic for β-spodumene structures. The body LAS2 of β-eucryptite solid-solution [Fig. 7(c) and (d)] resembles that of β-eucryptite but with finer grain morphology and more glassy matrix. Several closed pores are seen [Fig. 7(a) and (b)] in LAS1 with few large ones. The fracture mode is predominantly intergranular, though some evidence of transgranular fracture could be observed. The body LAS2 (the solid-solution) possesses numerous but very small closed pores [Fig. 7(c)] in a translucent glassy matrix with clear grain boundaries [Fig. 7(d)] of islands of crystals embedded in. Mixed inter- and transgranular fracture could be distinguished. The grains in β-spodumene are separated, having larger size [Fig. 7(e)] with some pores inside [Fig. 7(f)]. Cracks were noted to propagate from grain to grain[20] when the glassy matrix has higher thermal expansion than the crystalline inclusions, which are seen here with higher lithia content. The influence of porosity as a second phase on fracture behaviour is reflected as fracture fronts are induced to intersect these defects. The mode of fracture is affected by true porosities, their percents and sizes. The increased silica content and the change from hexagonal to tetragonal symmetry are reflected as increased true density according to the order LAS1 > LAS2 > LAS3, i.e. 2.4, 2.38 and 2.68 g/cm^3, respectively. The true porosity (in %) is at a minimum for the solid-solution, calculated values being 8.33, 5.46 and 23.88% for LAS1, LAS2 and LAS3, respectively.

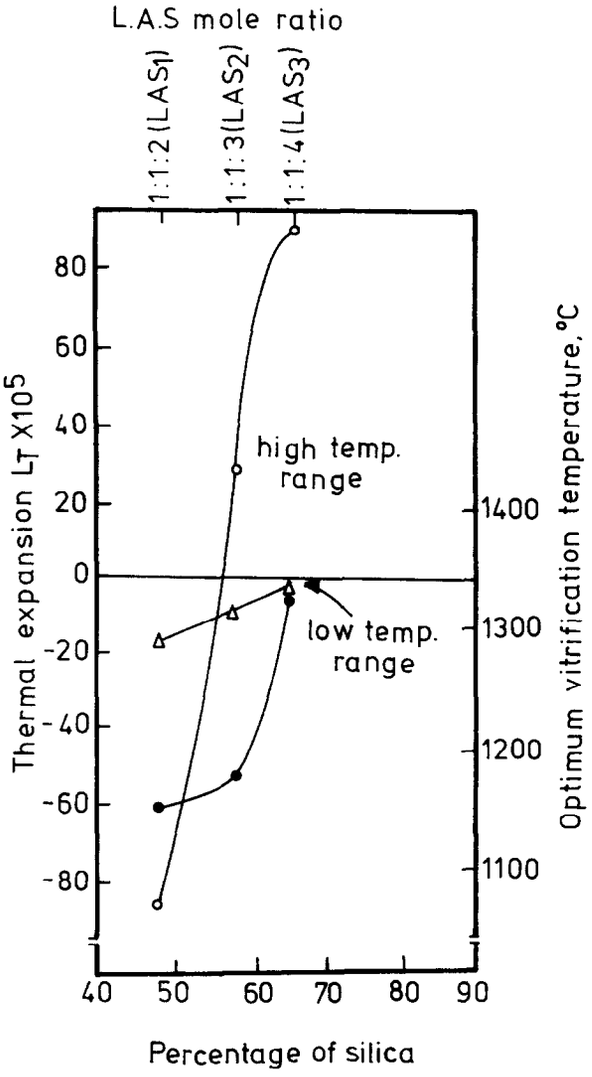

Fig. 6. Change of zero expansion wih lithia:alumina:silica ratios.

3.4.2 Powder structure

The SAED of LAS1 revealed a pollycrystalline structure as indicated by the well developed rings [Fig. 8(a)]. A lower order of crystallinity is indicated in LAS2 by the diffuse rings [Fig. 8(b)]. The larger glass core detected coincides with its smaller crystallite size [Fig. 7(b)], which was recently reported on the basis of X-ray line broadening.[18] Diffuse rings are also shown in the LAS3 body but with a much smaller glass halo [Fig. 3(c)].

Increased true density of the LAS bodies parallels increased silica at the expense of both lithium and aluminium oxides. However, the increased silica kept the structure open and the more siliceous glassy phase failed to produce fully vitrified bodies, therefore affecting the developed microtopography and making the mode of fracture transgranular.

4 CONCLUSIONS

The following conclusions can be drawn from the work described above.

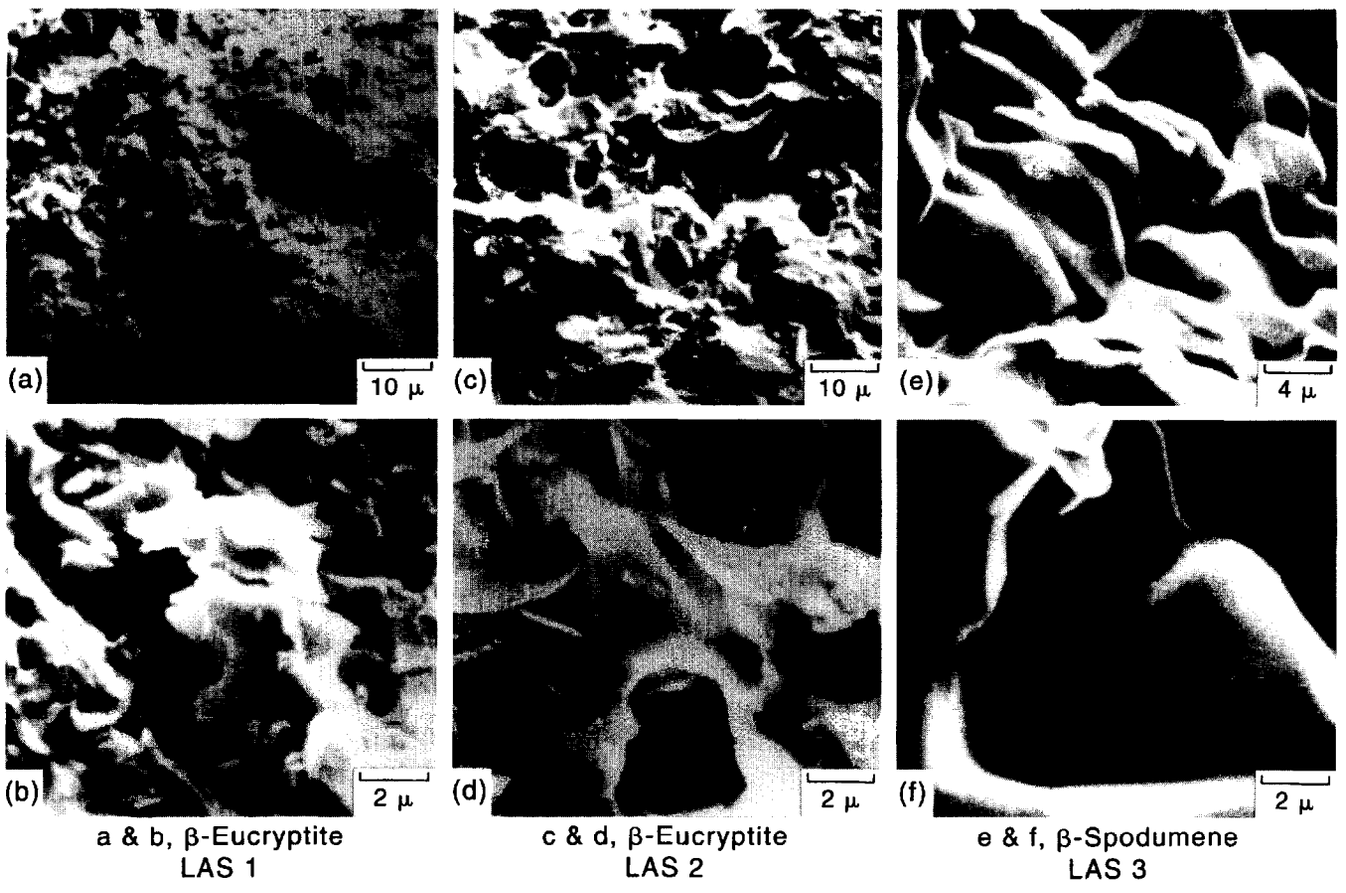

Fig. 7. SEM surface topography of the lithia ceramics.

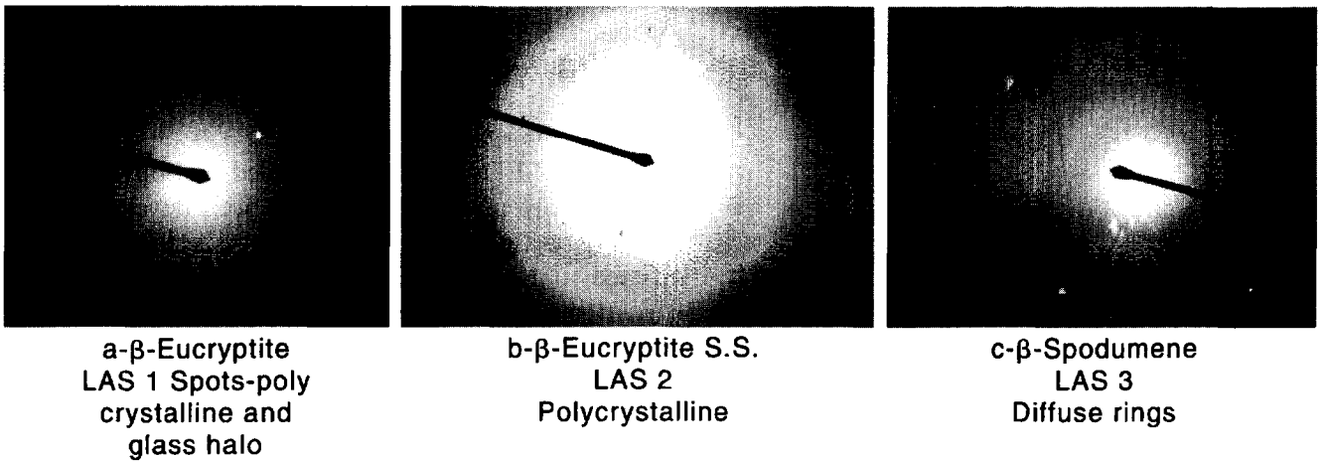

Fig. 8. SAED of lithia ceramic powders.

- Increasing the silica content of the LAS bodies at the expense of both lithia and alumina raised their densification temperatures and resulted in porous ceramic bodies.
- The change of crystalline structure from hexagonal β-eucryptite to tetragonal β-spodumene through solid-solution β-eucryptite is characterized by splitting and multiplicity of hydroxy IR-bands in parallel with shifts in position of the $(AlO_4)^-$ and $(AlO_6)^-$ bands.
- β-Eucryptite showed negative expansion up to 1000 °C. Changing to β-spodumene changed negative expansion to positive at temperatures which are composition dependent.
- Fracture fronts interacting with porosity are clearer in β-eucryptite bodies with higher thermal mismatch. Less viscous glassy phase is indicated by thermal expansion turnings at high temperature and the SAED glass halo in β-eucryptite solid-solution.

- The selection of which of the three ceramic bodies would be the best for Li-breeder would depend greatly on their response to fast neutron irradiation.

REFERENCES

1. PASCUCCI, M. R. & KATZ, R. N., *Interceram.*, **42** (1993) 2.
2. ABDELLAH, R., Effect of radiation on the physical properties of ceramic bodies and its use in dosimetry. PhD, Phys. Department, Faculty of Science, Cairo University, Egypt, 1987.
3. ALVANI, C. & CASADIO, S., Ceramics Today Ceramics Tomorrow. In *7th Cimtec World Ceramic Congress*, 24–30 June 1990.
4. WINKLER, H. G. F., *Acta Cryst.*, **1**(1) (1948) 27.
5. GRUHER, J. W., *Am. Mineralogist*, **33**(11-12) (1948) 679.
6. RUSTUM, R. & OBSORN, E. F., *J. Am. Ceram. Soc.*, **32**(6) (1949) 2086.
7. WHITE, R. P. & RIGBY, G. R., *Trans. Brit. Ceram. Soc.*, **53** (1954) 324.
8. HOBBS, L. W., *J. Am. Ceram. Soc.*, **62**(5-6) (1979) 267.
9. KREIDEL, N. J., *Ceramics in Severe Environments*, Materials Science Research Vol. 5, ed. W. Wurth Kreidel & H. Palmour III. Plenum Press, New York, 1971, p. 5.
10. RIEGER, W., *Thayngen, Sprechsaal*, **115**(12) (1982) 1102–1107.
11. ROY, R. B. & OBSORN, E. F., *J. Am. Ceram. Soc.*, **33**(5) (1950) 152.
12. GADSDEN, J. A., *Infrared Spectra of Minerals and Inorganic Compounds*. Butterworth, London, 1975, p. 16.
13. TARTE, P., *Spectrochim. Acta*, **20** (1964) 388.
14. BATES, J. B., DUDNEY, N. J., BROWN, O. M., WANG, J. C. & FECH, F. R., *J. Chem. Phys.*, **77**(10) (1982) 4838.
15. JOHANSON, R. T., BIEFELD, R. M., KNOTEK, M. L. & MOROSIN, B., *J. Electrochem. Soc.*, **123**(5) (1976) 680–687.
16. SCHULZ, H. J., *J. Am. Ceram. Soc.*, **57**(7) (1974) 313.
17. PILLARS, W. W. & PEACOR, D. R., *Am. Mineralogist*, **58** (1973) 38.
18. ABDELLAH, R., EL-SHAABINY, A. M., ABDEL FATTAH, W. I., RAMADAN, A. A. & FADEL, M. A., *Bull. Fac. Sc. Zagazig Univ.*, **9** (1987) 486–500.
19. HUMMEL, F. A., *J. Am. Ceram. Soc.*, **34**(8) (1951) 235.
20. BINNS, D. B., *Science of Ceramics, Vol. 1*, ed. G. H. Stewart. Academic Press, New York, 1962, p. 315.